

E-MRS Spring Meeting 2015 Symposium C - Advanced inorganic materials and structures for photovoltaics

Behavior of Photo Induced Minority Carrier Lifetime in PN Junction with Different Bias Voltages

T. Sameshima* and M. Hasumi

Tokyo University of Agriculture and Technology, Koganei, Tokyo 184-8588, Japan

Abstract

We report analysis of the photo-induced minority carrier effective lifetime (τ_{eff}) in a p^+n junction formed on the top surfaces of a n -type silicon substrate by ion implantation of boron and phosphorus atoms at the top and bottom surfaces followed by activation by microwave heating. Bias voltages were applied to the p^+ boron-doped surface with n^+ phosphorus-doped surface kept at 0 V. The values of τ_{eff} were lower than 1×10^{-5} s under the reverse-bias condition. On the other hand, τ_{eff} markedly increased to 1.4×10^{-4} s as the forward bias voltage increased to 0.7 V and then it levelled off when continuous-wave 635 nm light was illuminated at 0.74 mW/cm² on the p^+ surface. The carrier annihilation velocity S_{p^+} at the p^+ surface region decreased from 4000 to 265 cm/s as the forward bias voltage increased from 0 to 0.7 V. τ_{eff} also increased from 1.4×10^{-5} to 1.0×10^{-4} s as the intensity of 635 nm light increased from 0.04 to 0.74 mW/cm² under the open-circuit condition.

© 2015 Published by Elsevier Ltd. This is an open access article under the CC BY-NC-ND license (<http://creativecommons.org/licenses/by-nc-nd/4.0/>).

Peer-review under responsibility of The European Materials Research Society (E-MRS)

Keywords: minority carrier lifetime; pn junction; bias; carrier annihilation velocity

1. Introduction

The pn junction is an elementary structure for solar cells, photosensors and transistors [1-4]. The incorporation of impurities at the lattice sites is an essential process technology to form pn junctions. However, it may simultaneously cause photo-induced carrier annihilation defects, which limit the photo-induced carrier lifetime (τ_{eff}). Many passivation technologies have been developed to reduce the density of defects, such as hydrogenation and H₂O vapour heat treatment [5-6]. Measurement and analysis methods of τ_{eff} have also been developed to investigate photo-induced

* Corresponding author. Tel.: +81-42-388-7109 ; fax: +81-42-388-7109 .

E-mail address: tsamesim@cc.tuat.ac.jp

carrier annihilation defects such as measurements of the quasi-steady-state photoconductance (QSSPC), microwave photoconductive decay, and microwave absorption of photo-induced carriers caused by continuous light illumination [7-10]. We have recently reported that τ_{eff} changed with a bias voltage for a metal-oxide semiconductor (MOS) structure in crystalline silicon [11]. The experimental results suggest that the internal built-in potential distribution can change the probability of photo-induced minority carrier annihilation.

In this paper, we report an investigation of the annihilation properties of photo-induced minority carriers for a *pn* junction formed in crystalline silicon under the application of bias voltage. We demonstrate a marked change in τ_{eff} from 10^{-6} to 10^{-4} s in the case of light illumination on the surface of the *pn* junction as a bias voltage is applied from negative (reverse bias) to positive voltages (forward bias). We discuss the field-induced carrier annihilation in the p^+ region, and carrier annihilation velocity is numerically estimated. We also demonstrate increase in τ_{eff} with increasing the intensity of light under the condition of the open circuit voltage.

2. Experimental procedure

Figure 1 shows a schematic of the sample fabrication steps. $17\ \Omega\text{cm}$ *n*-type silicon substrates with a thickness of 500 μm and a crystalline orientation of (100) were prepared. The substrates were coated with 100-nm-thick thermally grown SiO_2 layers by heating in a wet atmosphere at $1100\ ^\circ\text{C}$. The ion implantation of boron atoms was conducted for the top surface of the silicon substrates. The acceleration energy was set at 25 keV to obtain the peak concentration at the interface of the thermally grown SiO_2 and silicon. The total dose was $2.0 \times 10^{15}\ \text{cm}^{-2}$. Boron atoms at a concentration of $1.0 \times 10^{15}\ \text{cm}^{-2}$ were effectively implanted in the silicon substrates. The ion implantation of phosphorus atoms at 75 keV was also conducted for the rear surface of the silicon substrates. Phosphorus atoms at a concentration of $1.0 \times 10^{15}\ \text{cm}^{-2}$ were effectively implanted in the silicon substrates. Most of boron and phosphorus atoms were located within 60 nm from the silicon surfaces. The implanted samples with the SiO_2 layers coated on the surfaces were subsequently heated by microwave irradiation using a commercial 2.45 GHz microwave oven at 1000 W for a duration of 150 s [12]. The samples were completely covered with carbon powders 2- μm -diameter for effective heating and placed on a quartz glass substrate with low heat conductivity to keep the heat energy in the sample region. The SiO_2 layers prevented the incorporation of other materials such as carbon into silicon. The SiO_2 layers were then removed by dipping the samples in 5% dilute hydrofluoric acid. Al electrodes were subsequently formed at the top and rear surfaces to enable the application bias voltages to the samples. The Al electrodes had a loop shape with an open middle area of $2.3\ \text{cm}^2$ for microwave transmission measurements.

Optical reflectivity spectra were measured between 250 and 1000 nm using a conventional spectrometer to investigate the crystalline volume ratio X_c in the ion-implanted surface regions. The SiO_2 layers were removed for precise measurement. The spectra were analysed using a numerical calculation program, which was constructed on the basis of the optical interference effect for an air/multiple Si layers/Si substrate structure [13]. The optical reflectivity

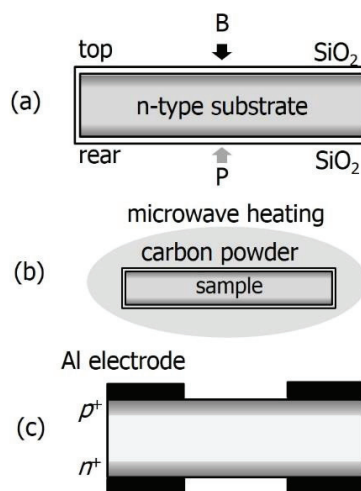


Fig. 1. Schematic sample fabrication steps of (a) boron and phosphorus ion implantations, (b) microwave heating, and (c) SiO_2 etching followed by Al electrode formation.

on the silicon surface depends on the complex refractive index of each silicon layer. Using the effective dielectric model, the complex refractive index with the crystalline volume ratio X_c is determined by combining the crystalline refractive index with the amorphous refractive index [14]. The thickness and crystalline volume ratio were changed for each layer to calculate the reflectivity. The most probable in-depth distribution of the crystalline volume ratio was obtained by fitting the calculated reflectivity spectra to the experimental reflectivity spectra.

To investigate the carrier lifetime and carrier annihilation probability as a function of the bias voltage, we used a 9.35-GHz-microwave-transmittance measurement system, as shown schematically in Fig. 2 [10,15]. The system had waveguide tubes, which had a narrow gap where a sample was placed. Continuous-wave (CW) 635 and 980 nm laser diode (LD) lights were introduced into the waveguide tubes. The light intensities were set at 0.74 and 0.48 mW/cm² on the sample surface for 635 and 980 nm lights, respectively, to realize the same photon flux between the two different wavelengths. The penetration depth was about 2.7 and 120 μm for 635 and 980 nm lights, respectively [25]. The microwave transmittances in a dark field T_d , under the light illumination of the top boron-implanted surface T_p (top) and rear phosphorus-implanted surface T_p (rear) were precisely measured with different bias voltages applied to the Al electrode formed on the p^+ surface while the Al electrode formed on the n^+ surface at 0 V. T_d , T_p (top), T_p (rear) were analysed with our finite-element numerical calculation program with a Fresnel-type microwave interference effect between silicon surfaces to obtain the photo-induced minority carrier effective lifetime τ_{eff} (top) and τ_{eff} (rear). The electrical current density was also measured as a function of bias voltage. τ_{eff} (top) was also measured with different intensity of 635-nm light ranging from 0.04 to 0.74 mW/cm² under the open circuit voltage.

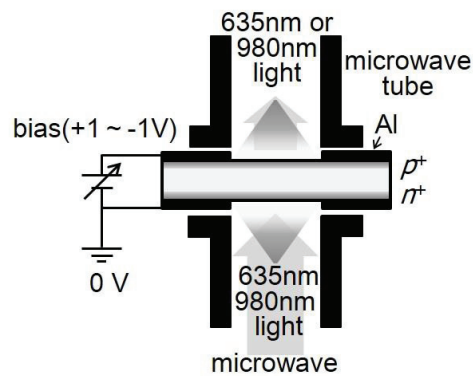


Fig. 2. Schematic 9.35-GHz-microwave-transmittance measurement system.

3. Results and discussion

Figure 3 shows experimental optical reflectivity spectra of the (a) initial, as-boron-, and phosphorus-ion-implanted surfaces and (b) microwave heated boron- and phosphorus-ion implanted surfaces. The SiO₂ layers were removed for all samples for precise measurements. Two large peaks of E_1 and E_2 caused by the large joint density of states at the X point in the Brillouin zone of crystalline silicon appeared at 340 and 275 nm for the initial sample. On the other hand, the peak heights of E_1 and E_2 became small upon boron ion implantation. Decreases in the heights of the peaks indicate the partial amorphization of the surface region for the boron-implanted surface. Moreover, no E_1 and E_2 peaks were observed in the case of phosphorus implantation, as shown in Fig. 3(a). Phosphorus implantation caused complete amorphization of the surface region. On the other hand, the microwave heating changed the optical reflectivity spectra of the ion-implanted samples to similar to the optical reflectivity spectrum of the initial sample having the E_1 and E_2 peaks, as shown in Fig. 3(b). The amorphized surface regions were recrystallized by the microwave heating. Analysis of the reflectivity spectra indicated that the boron ion implantation decreased X_c to 0.3 in the top 5 nm region and 0.95 from a depth of 5 to 40 nm because of boron implantation with a high peak concentration of $3 \times 10^{20} \text{ cm}^{-3}$. The phosphorus ion implantation decreased X_c to 0.0 in the top 35 nm region and 0.7 from a depth of 35 to 50 nm. On the other hand, the microwave heating at 1000 W for 150 s increased X_c to 1.0 in the boron- and phosphorus-implanted surface regions. The microwave heating effectively recrystallized the silicon surface regions.

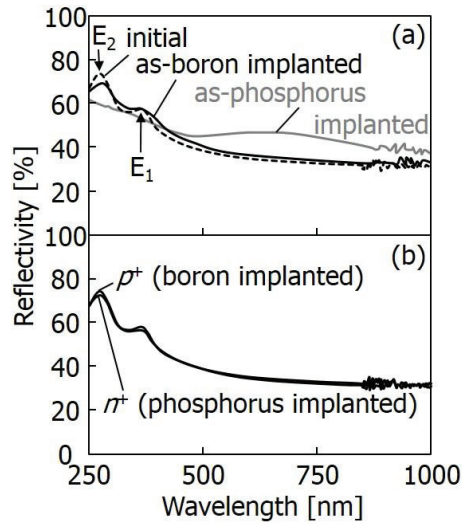


Fig. 3. Experimental optical reflectivity spectra of (a) initial, as-boron- and phosphorus-ion implanted surfaces and (b) microwave heated boron- and phosphorus-ion implanted surfaces.

The initial sample had a microwave transmissivity in a dark field T_d of 26.1% because of the high resistivity of 17 Ωcm of the silicon substrate. The majority carrier concentration and the Fermi level were estimated to be $2.8 \times 10^{14} \text{ cm}^{-3}$ and 0.826 eV, respectively, from the valence band edge. T_d was not changed by boron and phosphorus implantation because carriers were not generated in the as-implanted state. On the other hand, T_d was markedly decreased to 6.8% by the microwave heating. Carriers generated by the activation of boron- and phosphorus-doped surface regions caused substantial absorption of the incident microwaves. The analysis of T_d indicated that the sheet resistivity decreased from 340 (initial) to 88 Ω/sq . Doped surface regions with low resistivities were successfully formed by the microwave heating.

Figure 4 shows τ_{eff} (top) and τ_{eff} (rear) in the cases of light illumination at 635 nm (open circles) and 980 nm (solid circles) as a function of the bias voltage applied to the Al electrodes formed at the p^+ regions while keeping the Al electrodes formed in the n^+ regions at 0 V. τ_{eff} (top) was lower than 1×10^{-5} s for the bias voltage of lower than 0 V (reverse-bias condition) in the case of 635 nm light illumination. It markedly increased to 1.4×10^{-4} s as the bias voltage increased from 0 to 0.7 V (forward bias condition) and levelled off above 0.7 V. On the other hand, τ_{eff} (top) ranged from 3.1×10^{-5} to 3.9×10^{-5} s lower than 0 V or 0 V in the case of the 980 nm light illumination. These values were higher than those in the case of 635 nm light illumination. τ_{eff} (top) in the case of 980 nm light illumination increased to

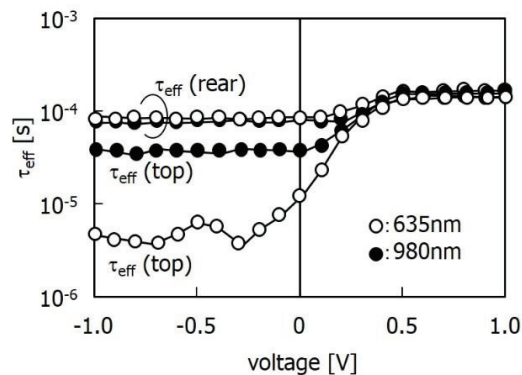


Fig. 4. τ_{eff} (top) and τ_{eff} (rear) in the cases of light illumination at 635 (open circles) and 980 nm (solid circles) as a function of the bias voltage applied to the Al electrodes formed at the p^+ regions with keeping the Al electrodes formed at the n^+ regions at 0 V.

1.5×10^{-4} s as the bias voltage increased from 0 to 0.7 V and levelled off above 0.7 V. When 635 nm light was illuminated on the n^+ surfaces, τ_{eff} (rear) ranged from 8.1×10^{-5} to 8.4×10^{-5} s for a bias voltage lower than 0 V or 0 V, in contrast to the low τ_{eff} (top) in the case of 635 nm light illumination. τ_{eff} (rear) increased to 1.6×10^{-4} s as the bias voltage increased from 0 to 0.7 V and levelled off above 0.7 V. τ_{eff} (rear) in the case of 980 nm light illumination had a similar behaviour to τ_{eff} (rear) in the case of 635 nm light illumination. τ_{eff} (rear) ranged from 7.4×10^{-5} to 7.7×10^{-5} s for a bias voltage of lower than 0 V or at 0 V. It increased to 1.5×10^{-4} s as the bias voltage increased from 0 to 0.7 V and levelled off above 0.7 V. The results in Fig. 4 suggest that τ_{eff} was sensitive to the electrical-field effect caused by the applied voltage. τ_{eff} (top) had a small value of lower than 1×10^{-5} s only in the case of 635 nm light illumination under the reverse-bias condition. On the other hand, the application of a sufficiently high forward bias voltage resulted in τ_{eff} having similar values ranging from 1.4×10^{-4} to 1.6×10^{-4} s among four light illumination modes.

Figure 5 shows (a) the electrical current density as a function of applied voltage (J-V) under the conditions of a dark field and 635 and 980 nm light illumination of the top p^+ surfaces and (b) a magnification of the J-V characteristics in the negative current region. Rectified diode characteristics are observed for every case. The results in Fig. 5 therefore show that an internal potential barrier was formed by the p^+ -doped region in the n -type substrates. Similar photo-induced negative current characteristics were observed for bias ranging from -1 to 0.35 V under 635 and 980 nm light illumination with short circuit currents J_{sc} of -1.37×10^{-3} and -1.36×10^{-3} Acm^{-2} , respectively. A photo-induced current and the photovoltaic effect were observed. Similar I-V characteristics were obtained in the cases of the 635 and 980 nm light illumination of the rear n^+ surface, while J_{sc} was slightly low of -1.0×10^{-3} and -1.04×10^{-3} Acm^{-2} .

The results in Fig. 4 clearly show that τ_{eff} strongly depended on the bias voltage. Low values of τ_{eff} were observed for every illumination mode under the conditions of reverse or zero bias voltage, which are associated with the high built-in potential barrier formed under the p^+ -doped region. In particular, the values of τ_{eff} (top) in the case of the 635 nm light illumination case were very low, 1.2×10^{-5} s or lower. On the other hand, application of the forward bias voltage increased τ_{eff} . τ_{eff} (top) in the case of 635 nm light illumination case markedly increased to 1.4×10^{-4} s. τ_{eff} had similar values ranging from 1.4×10^{-5} to 1.6×10^{-6} s among the four illumination modes above a forward bias of 0.7 V. A built-in potential was formed in the p^+n junction region at a bias of 0 V in this samples. There were a positively charged region in the depletion region and negatively charged-up region in the p^+ region adjacent to the interface of the p^+n junction. According to the classical theory [16], the quasi-Fermi potential of the photo-induced hole minority carriers was almost constant over the depletion region because the photo-induced current density was low, 1.4×10^{-3} Acm^{-2} , at a bias of 0 V, under the present experimental conditions. Therefore the diffusion of photo-induced hole minority carriers can be considered to satisfy the flat band condition in the depletion region. We used a finite-element numerical calculation program that included the theories of carrier generation associated with the optical absorption coefficients as well as carrier diffusion between the two p^+/n and n/n^+ interfaces, where the annihilation velocities S_{p^+} and S_{n^+} were

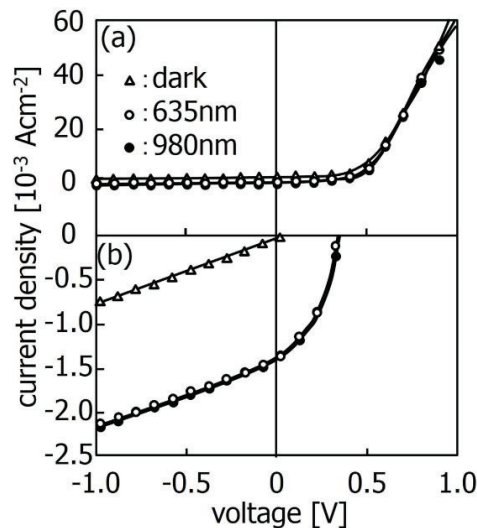


Fig.5. (a) electrical current density as a function of applied voltage (J-V) in the conditions of the dark field, 635 and 980 nm light illumination of the p^+ surfaces and (b) magnifications of J-V characteristics for the negative current region.

set at the p^+/n and n/n^+ interfaces [17]. The density of photo-induced minority carriers as a function of the depth x from the p^+/n interface in the steady state under the illumination of the p^+ region with CW light is given as

$$D \frac{\partial^2 n_m(x)}{\partial x^2} + \frac{n_m(x)}{\tau_b} - g(x) = 0 \tag{1}$$

where τ_b , $n_m(x)$, $g(x)$, and D are the bulk lifetime, the carrier volume density, the carrier generation rate at a depth of x , and the diffusion constant, respectively. Carrier generation occurs in the substrate bulk and which depends on the optical absorption coefficient at a certain light wavelength. $g(x)$ is given with the optical penetration depth d of light as

$$g(x) = \frac{G}{d} e^{-\frac{x}{d}} \tag{2}$$

The boundary conditions are given as

$$D \left. \frac{\partial n_m(x)}{\partial x} \right|_{x=0} = S_{p^+}(V) n_m(0) - g(0) \Delta x \tag{3a}$$

$$D \left. \frac{\partial n_m(x)}{\partial x} \right|_{x=L} = -S_{n^+} n_m(L) - g(L) \Delta x \tag{3b}$$

where L is the thickness of the semiconductor substrate between the p^+/n and n/n^+ interfaces of and Δx is the unit lattice length for 2×10^{-5} cm in the present calculation. n_m was obtained by the integration of $n_m(x)$ from 0 to L . τ_{eff} was obtained from calculated by dividing the n_m by G . We assumed that an ohmic junction was formed at the n/n^+ interface and S_{n^+} was constant for every bias voltage. The most probable $S_{p^+}(V)$ and S_{n^+} as a function of bias voltage were analyzed by fitting calculated τ_{eff} to experimental τ_{eff} measured with four illumination modes. In the present cases, we assumed that τ_b was long enough, and that carrier annihilation was governed only by the annihilation velocity at the surfaces.

Figure 6 shows $S_{p^+}(V)$ as a function of bias voltage. S_{n^+} is also presented by a solid line. $S_{p^+}(V)$ was high, ranging from 4000 to 7200 cm/s, under the conditions of reverse and zero bias voltage. It decreased to 265 cm/s, which was comparable to the value of S_{n^+} of 100 cm/s, as the bias voltage increased to 0.7 V. In general, the excess carrier annihilation rate is determined by the active carrier recombination defect density per unit area, the carrier capture crosssection, the carrier velocity and the excess electron and hole carrier densities [29,33-35]. In the present work, high values of $S_{p^+}(V)$ appeared under the application of the reverse and zero bias voltage, high built-in potential associated

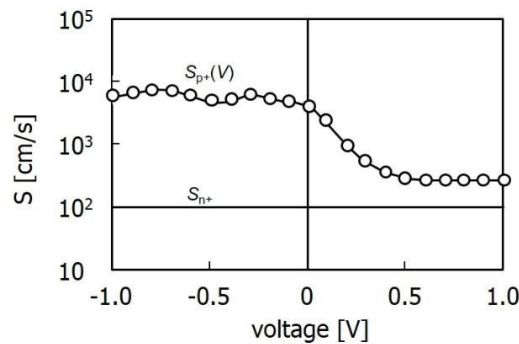


Fig. 6 The carrier annihilation velocity at the p^+ interface $S_{p^+}(V)$ as a function of bias voltage. The carrier annihilation velocity at the n^+ interface S_{n^+} is also presented by a solid line.

with the negative charging in the p^+ region and positive charging in the depletion region of the n -type substrate. We suggest that negative charging in the p^+ region increases $S_{p^+}(V)$ to a high value. There are many defect states in the band gap in the p^+ region because of the heavy doping. Under the neutral condition, the Fermi level locates close to the valence band edge. Most of the defect states are occupied and not active for carrier recombination. The negative charging increases the Fermi level to the deep level and is expected to increase the density of unoccupied and active defect states for carrier recombination [18]. The injected excess hole and electron carriers should be effectively recombined in the negatively charged region owing to the high density of active defects. The high $S_{p^+}(V)$ effectively decreased τ_{eff} (top) especially in the case of 635 nm light illumination because photo-induced carriers were generated near the p^+/n interface because of the low value of d of 2.7 μm . On the other hand, 980 nm light illumination resulted in photo-induced carriers in the region with d of 120 μm . τ_{eff} (top) maintained high values because of the time required for diffusion from the deep carrier generation region to the p^+ interface. Moreover, photo-induced carriers generated by light illumination of the n^+ region traversed across the silicon substrate to reach the p^+ interface. The long diffusion distance allowed high values of τ_{eff} (rear). On the other hand, the application of forward bias voltage reduces the negative charging in the p^+ region facing the pn junction. The Fermi level decreases to the valence edge, and defect states are expected to become occupied and inactive for carrier recombination. We believe that the reduction of negative charging in the p^+ region is the reason why the application of the forward bias voltage decreased $S_{p^+}(V)$. $S_{p^+}(V)$ is minimum when the negative charge density is negligible small. The lowest value of $S_{p^+}(V)$ of 265 cm^2/s at 0.7 V suggests that the flat band condition is established.

Light illumination reduces the height of the built-in potential because photo-induced electrons and holes compensate positive charges in the n -type substrate and negative charges in the p^+ region. High light intensity is effective to reduce the height of the built-in potential because of high density of photo-induced carriers. Figure 7 shows τ_{eff} (top) and τ_{eff} (rear) as a function of the light intensity of 635 nm light illumination under the open circuit condition. τ_{eff} (top) was a low value of 1.4×10^{-5} s at a low light intensity of 0.04 mW/cm^2 . This result indicates that high built-in potential maintained under the light illumination because charge compensation effect is low. Negative charging in the p^+ region increases S and decreased τ_{eff} (top). τ_{eff} (top) increased to 1.0×10^{-4} s as the light intensity increased to 0.74 mW/cm^2 . High light intensity generated a high density of photo-induced carriers, which effectively reduced the built-in potential and negative charging in the p^+ region. τ_{eff} (top) therefore increased under the open circuit condition. τ_{eff} (rear) also increased from 6.0×10^{-5} to 1.2×10^{-4} s as the light intensity increased from 0.04 to 0.74 mW/cm^2 because the n^+ surface had the low S_{n^+} and the long diffusion duration was required for photo-induced carriers to reach p^+ surface across the substrate. Changes in τ_{eff} (top) and τ_{eff} (rear) with the light intensity shown in Fig. 7 indicate internal field effect carrier annihilation.

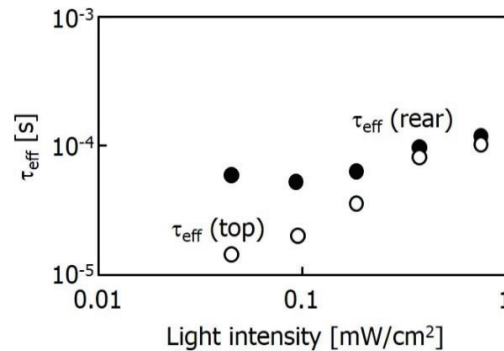


Fig. 7 τ_{eff} (top) and τ_{eff} (rear) in the case of light illumination at 635 nm as a function of the light intensity under the open circuit condition.

4. Conclusions

We reported an investigation of the annihilation properties of photo-induced minority carriers for a pn junction formed in n -type crystalline silicon substrates under the application of bias voltage. The p^+n junction was formed in the top surface region of the silicon substrates by boron and phosphorus ion implantation with a dose of $1 \times 10^{15} \text{ cm}^{-2}$

followed by microwave heating using a 2.45 GHz microwave oven at 1000 W for 150 s. The ion-implanted surface regions were recrystallized, and boron and phosphorus atoms were effectively activated with a sheet resistivity of 88 Ω/sq . Rectified characteristics, a photo induced current and the photo-voltaic effect were observed in the J-V characteristics under the application of reverse and forward bias voltages to the Al electrodes formed at the p^+ and n^+ surfaces. τ_{eff} (top) in the case of 635 nm light illumination was lower than 1×10^{-5} s for the reverse-bias condition, while it markedly increased to 1.4×10^{-4} s as the forward bias voltage increased from 0 to 0.7 V and the leveled off. On the other hand, τ_{eff} (top) ranged from 3.1×10^{-5} to 3.9×10^{-5} s for the reverse-bias condition in the case of the 980 nm light illumination. It increased to 1.5×10^{-4} s as the forward-bias voltage increased from 0 to 0.7 V and leveled off. τ_{eff} (rear) ranged from 8.1×10^{-5} to 8.4×10^{-5} s for the reverse bias condition in the cases of 635 nm light illumination, while it increased to 1.6×10^{-4} s as the forward bias voltage increased from 0 to 0.7 V and then leveled off. τ_{eff} (rear) ranged from 7.4×10^{-5} to 7.7×10^{-5} s for the reverse-bias condition in the case of 980 nm light illumination, while it increased to 1.6×10^{-4} s as the forward-bias voltage increased from 0 to 0.7 V and then leveled off. The numerical analysis of τ_{eff} (top) and τ_{eff} (rear) gave a high values of S_{p^+} (V) from 4000 to 7200 cm/s under the conditions of reverse and zero bias voltage, while it decreased to 265 cm/s, when the forward-bias voltage increased from 0 to 0.7 V and then leveled off under the assumption of a constant value of S_{n^+} of 100 cm/s. The high values of S_{p^+} (V) for the reverse-bias condition were interpreted to be due to an increase in the density of unoccupied and active defect states caused by electrical negative charging in the p^+ region. S_{p^+} (V) decreased to 265 cm/s, which was probably limited by the intrinsic density of defect states, when a forward-bias voltage of 0.7 V was applied. τ_{eff} (top) and τ_{eff} (rear) increased from 1.4×10^{-5} and 6.0×10^{-5} to 1.0×10^{-4} and 1.2×10^{-4} s, respectively, as the light intensity increased 0.04 to 0.74 mW/cm² in the case of 635 nm light illumination under the open circuit condition. Accumulation of photo-induced carriers generated by illumination with the high light intensity effectively reduced built-in potential and negative charging in the p^+ region so that S_{p^+} decreased and τ_{eff} increased.

Acknowledgements: This work was supported by Professor. J. H. Werner and by a Grants-in-Aid for Scientific Research C (No. 25420282) from the Ministry of Education, Culture, Sports, Science and Technology of Japan, Sameken Co., Ltd., and Japan Science and Technology Agency A-STEP (No. AS2621088J).

References

- [1] S. M. Sze, *Semiconductor Devices, physics and technology* (Wiley, New York, 1985) Chap 3
- [2] M. A. Green. The path to 25% silicon solar cell efficiency: History of silicon cell evolution. *Prog. Photovoltaics* 17, 183 (2009)
- [3] E. A. G. Webster, L. A. Grant, R. K. Henderson. Transient Single-Photon Avalanche Diode Operation, Minority Carrier Effects, and Bipolar Latch Up. *IEEE Trans. Electron Devices* 60, 1188 (2013)
- [4] M. Mehrotra, J. C. Hu, M. Rodder. A 1.2V, sub-0.09 μm gate length CMOS technology. IEDM '99. Technical Digest. International p. 419
- [5] I.-W. Wu, A. G. Lewis, T.-Y. Hung, A. Chiang. Effects of trap-state density reduction by plasma hydrogenation in low-temperature polysilicon TFT. *Electron Device Letters, IEEE* 10, 123 (1989)
- [6] K. Sakamoto, T. Sameshima. Passivation of SiO₂/Si Interfaces Using High-Pressure-H₂O-Vapor Heating. *Jpn. J. Appl. Phys.* 39, 2492 (2000).
- [7] G. S. Kousik, Z. G. Ling, P. K. Ajmera. Nondestructive technique to measure bulk lifetime and surface recombination velocities at the two surfaces by infrared absorption due to pulsed optical excitation. *J. Appl. Phys.* 72, 141 (1992)
- [8] J. M. Borrego, R. J. Gutmann, N. Jensen, O. Paz. Non-destructive lifetime measurement in silicon wafers by microwave reflection. *Solid-State Electron* 30, 195 (1987)
- [9] Y. Ogita. Bulk lifetime and surface recombination velocity measurement method in semiconductor wafers. *J. Appl. Phys.* 79, 6954 (1996)
- [10] T. Sameshima, H. Hayasaka, T. Haba. Analysis of Microwave Absorption Caused by Free Carriers in Silicon. *Jpn. J. Appl. Phys.* 48, 021204 (2009)
- [11] T. Sameshima, J. Furukawa, T. Nakamura, S. Shigeno, T. Node, S. Yoshidomi, M. Hasumi. Photo induced minority carrier annihilation at crystalline silicon surface in metal oxide semiconductor structure. *Jpn. J. Appl. Phys.* 53, 031301 (2014)
- [12] M. Hasumi, T. Nakamura, S. Yoshidomi, T. Sameshima. Activation of silicon implanted with phosphorus and boron atoms by microwave annealing with carbon powder as a heat source. *Jpn. J. Appl. Phys.* 53, 05FV05 (2014)
- [13] M. Born and E. Wolf, *Principles of Optics* (Pergamon, New York, 1974) Chaps. 1 and 13
- [14] E. D. Palk. *Handbook of Optical Constants of Solids* (Academic Press, London, 1988) p. 562 and 577
- [15] T. Sameshima, T. Nagao, S. Yoshidomi, K. Kogure, M. Hasumi. Minority Carrier Lifetime Measurements by Photoinduced Carrier Microwave Absorption Method. *Jpn. J. Appl. Phys.* 50, 03CA02 (2011)
- [16] Y. Taur, T. Ning. *Fundamentals of Modern VLSI Devices* (Cambridge University Press, Cambridge, U. K. 1998) Chap. 2
- [17] T. Sameshima, S. Shibata. Annihilation of photo induced minority carrier caused by ion implantation and rapid thermal annealing. *Jpn. J. Appl. Phys.* 53, 061301 (2014)
- [18] A. S. Groove. *Physics and Technology of Semiconductor Devices* (Wiley, New York, 1967) Chap. 5